

ACCRETION ONTO BLACK HOLES FROM LARGE SCALES REGULATED BY RADIATIVE FEEDBACK. III. ENHANCED LUMINOSITY OF INTERMEDIATE MASS BLACK HOLES MOVING AT SUPERSONIC SPEEDS

KWANGHO PARK¹ AND MASSIMO RICOTTI²

Department of Astronomy, University of Maryland, College Park, MD 20740, USA

(Received; Accepted)

Draft version November 10, 2018

ABSTRACT

In this third paper of a series, we study the growth and luminosity of black holes (BHs) in motion with respect to their surrounding medium. We run a large set of two-dimensional axis-symmetric simulations to explore a large parameter space of initial conditions and formulate an analytical model for the accretion. Contrary to the case without radiation feedback, the accretion rate increases with increasing BH velocity v_{bh} reaching a maximum value at $v_{\text{bh}} = 2c_{\text{s,in}} \sim 50 \text{ km s}^{-1}$, where $c_{\text{s,in}}$ is the sound speed inside the “cometary-shaped” H II region around the BH, before decreasing as v_{bh}^{-3} when the ionization front (I-front) becomes R -type (rarefied) and the accretion rate approaches the classical Bondi–Hoyle–Lyttleton solution. The increase of the accretion rate with v_{bh} is produced by the formation of a D -type (dense) I-front preceded by a standing bow-shock that reduces the downstream gas velocity to transonic values. There is a range of densities and velocities where the dense shell is unstable producing periodic accretion rate peaks which can significantly increase the detectability of intermediate-mass BHs. We find that the mean accretion rate for a moving BH is larger than that of a stationary BH of the same mass if the medium temperature is $T_{\infty} < 10^4 \text{ K}$. This result could be important for the growth of seed BHs in the multi-phase medium of the first galaxies and for building and early X-ray background that may affect the formation of the first galaxies and the reionization process.

Subject headings: accretion, accretion disks – black hole physics – dark ages, reionization, first stars – hydrodynamics – methods: numerical – radiative transfer

1. INTRODUCTION

Gravitationally driven gas inflow onto moving point masses such as black holes (BHs) or neutron stars has been described analytically in the 1940s by Bondi–Hoyle–Lyttleton (Hoyle & Lyttleton 1939; Bondi & Hoyle 1944; Bondi 1952). The generalized formula for the accretion onto a point mass moving with velocity v_{bh} is obtained from the Bondi formula by replacing the gas sound speed, $c_{\text{s},\infty}$, with an effective speed $v_{\text{eff}} = (c_{\text{s},\infty}^2 + v_{\text{bh}}^2)^{1/2}$. The accretion rate $\dot{M} \propto \rho v_{\text{eff}} \sigma_{\text{eff}}$ is roughly estimated as the gas flux through the effective cross section $\sigma_{\text{eff}} = \pi r_{\text{eff}}^2$, where $r_{\text{eff}} = GM_{\text{bh}}/v_{\text{eff}}^2$ is the distance at which the escape velocity of the gas equals v_{eff} . Despite the similarities between the Bondi and Lyttleton formulae, in the second case the accretion onto the BH is not spherically symmetric: most of the gas streams past the BH and is gravitationally focused on the axis of symmetry of the problem. The component of the gas velocity perpendicular to the direction of the BH motion is converted into thermal energy and is mostly dissipated, thus a fraction of the gas becomes gravitationally bound to the BH and is accreted from the downstream direction. The generalized Bondi–Hoyle–Lyttleton formula is

$$\dot{M}_{\text{BHL}} = \frac{\dot{M}_B}{(1 + v_{\text{bh}}^2/c_{\text{s},\infty}^2)^{3/2}}, \quad (1)$$

where \dot{M}_B is the Bondi accretion rate onto non-moving BHs $\dot{M}_B = \pi e^{3/2} \rho_{\infty} G^2 M_{\text{bh}}^2 c_{\text{s},\infty}^{-3}$ (assuming isothermal equation of state: $\gamma = 1$). Here, M_{bh} is the BH mass, and

ρ_{∞} is the density of the ambient gas. The term in the denominator of Equation (1) is the only term that accounts for the motion of the point mass, thus for supersonic BH motion the accretion rate decreases with increasing velocity as v_{bh}^{-3} . Numerical simulations of accretion onto moving BHs have confirmed the validity of the Lyttleton equation (Shima et al. 1985; Ruffert & Arnett 1994; Ruffert 1996), even in the presence of non-axisymmetric flows that necessarily arise in three-dimensional simulations due to hydrodynamical instabilities (Cowie 1977; Matsuda et al. 1987; Fryxell & Taam 1988; Taam & Fryxell 1988; Soker 1990; Koide et al. 1991; Livio et al. 1991; Foglizzo & Ruffert 1997, 1999; Foglizzo et al. 2005).

For the case of accretion onto stationary BHs, the radiation emitted near the gravitational radius of the BH typically reduces the rate of gas supply to the BH from large scales well below the value given by the Bondi formula. This is because X-ray and UV heating increases the sound speed of the gas in the proximity of the BH (Ostriker, Weaver, Yahil, & McCray 1976; Cowie, Ostriker, & Stark 1978; Bisnovatyi-Kogan & Blinnikov 1980; Krolik & London 1983; Vitello 1984; Wandel, Yahil, & Milgrom 1984; Ostriker, Choi, Ciotti, Novak, & Proga 2010), and because radiation pressure accelerates the gas and dust away from the BH (Shapiro 1973; Ostriker, Weaver, Yahil, & McCray 1976; Begelman 1985; Ricotti, Ostriker, & Mack 2008). Indeed, the maximum accretion rate that can be achieved in most cases is the Eddington rate. In this limit, the outward acceleration of the gas due to Compton scattering of radiation with free electrons equals the inward gravitational acceleration. For supermassive BHs (SMBHs), the picture is far more complex because the hot ionized region and the Bondi radius extend to galactic scales. Thus, it is necessary to model the evolution of the host galaxy, with its stellar populations and the interstel-

kpark@astro.umd.edu, ricotti@astro.umd.edu

¹ McWilliams Center for Cosmology, Carnegie Mellon University, Pittsburgh, PA 15213, USA

² Joint Space-Science Institute (JSI), College Park, MD 20742, USA

lar medium (ISM) in addition to the accreting SMBH. Despite the complexity of this problem, a significant amount of work exists in the literature on the self-regulation mechanisms for the growth of SMBHs at the centers of elliptical galaxies (Ciotti & Ostriker 2001; Sazonov, Ostriker, Ciotti, & Sunyaev 2005; Ciotti & Ostriker 2007; Ciotti, Ostriker, & Proga 2009; Lusso & Ciotti 2011; Novak, Ostriker, & Ciotti 2011, 2012), for radiation-driven axis-symmetric outflows in active galactic nuclei (Proga 2007; Proga, Ostriker, & Kurosawa 2008; Kurosawa, Proga, & Nagamine 2009; Kurosawa & Proga 2009a,b) and more generally on the co-evolution of galaxies and their SMBHs. The study of the cosmological origin and growth of SMBHs is a multi-scale problem often approached using large-scale simulations. Typically, the limited resolution of these cosmological simulations precludes resolving the SMBH Bondi radius, hence, the accretion rate is modeled using sub-grid recipes largely based on the Eddington-limited Bondi formula (Volonteri & Rees 2005; Pelupessy, Di Matteo, & Ciardi 2007; Greif, Johnson, Klessen, & Bromm 2008; Alvarez, Wise, & Abel 2009; Kim, Wise, Alvarez, & Abel 2011; Blecha, Cox, Loeb, & Hernquist 2011; Blecha, Loeb, & Narayan 2013), sometimes with the introduction of a normalization parameter for the accretion rate to match observations (Di Matteo et al. 2005; Springel et al. 2005; Di Matteo et al. 2008).

Recently, there has been renewed interest on studies of accretion onto intermediate mass BHs (IMBHs; Milosavljević et al. 2009a,b; Park & Ricotti 2011; Li 2011; Park & Ricotti 2012), motivated by observations of ultraluminous X-ray sources (ULXs) in nearby galaxies (for a review Miller & Colbert 2004; van der Marel 2004), and in the early universe, because some simulations predict formation of IMBHs as Population III star remnants (Abel, Anninos, Norman, & Zhang 1998; Bromm, Coppi, & Larson 1999; Abel, Bryan, & Norman 2000; Madau & Rees 2001; Schneider, Ferrara, Natarajan, & Omukai 2002; Oh & Haiman 2002; Whalen & Fryer 2012; Jeon, Pawlik, Greif, Glover, Bromm, Milosavljević, & Klessen 2012; Johnson, Whalen, Fryer, & Li 2012a; Stacy, Greif, & Bromm 2012) or from direct collapse of quasi-stars (Carr, Bond, & Arnett 1984; Haehnelt, Natarajan, & Rees 1998; Fryer, Woosley, & Heger 2001; Begelman, Volonteri, & Rees 2006; Volonteri, Lodato, & Natarajan 2008; Omukai, Schneider, & Haiman 2008; Regan & Haehnelt 2009; Mayer, Kazantzidis, Escala, & Callegari 2010; Johnson, Khochfar, Greif, & Durier 2011; Johnson, Whalen, Li, & Holz 2012b).

Our previous work in this series (Park & Ricotti 2011, 2012, hereafter Papers I and II, respectively) has been partially motivated by the need to better describe the sub-grid recipe for accretion onto IMBH (and SMBH, with some caveats) in large-scale cosmological simulations. We have taken the most basic approach to understanding the growth of IMBHs and SMBHs, focusing on the fundamental problem of Bondi-type accretion (accretion from a homogeneous and isotropic gas) modified by a simple feedback loop that couples the accretion rate to the luminosity output: $L = \eta \dot{M} c^2$. The photon-gas coupling is due to isotropic emission of radiation from a central source, affecting the gas inflow through thermal and radiation pressures. We have started with idealized initial conditions, adding one physical process at a time, in order to understand and model analytically the modified Bondi problem for a large parameter space of initial conditions. One-dimensional and two-dimensional (2D) radiation-hydrodynamic simulations are used to explore the large parameter space of BH

masses, ambient gas density/temperature, radiative efficiency, and spectrum of the emitted radiation. We have then derived a physically motivated model for the BH growth and luminosity and provide analytic formulae that fully characterize the model. Despite the simplicity of the initial conditions, we found a rich phenomenology that can be described with a simple scaling arguments. The main results are: the mean accretion rate is proportional to the thermal pressure of the ambient gas and is always less than 1% of the Bondi rate. The accretion rate is periodic, with period of the luminosity bursts proportional to the average size of the ionized hot bubble and peak accretion rates about 10 times the mean. Most interestingly, we have discovered that there are two distinct modes of oscillations with very different duty cycles (6% and 50%), governed by two different depletion processes of the gas inside the ionized bubble (see Papers I and II).

This paper is the continuation of our previous work on characterizing how the Bondi-Lyttleton problem is modified by radiation feedback, but here we focus on the growth rate and luminosity of BHs in motion with respect to their surrounding medium: i.e., Lyttleton accretion modified by a radiative feedback loop. Considering the motion of the BH is important for the study of stellar BH (e.g., Wheeler & Johnson 2011) and IMBHs accreting from the ISM, both in the early universe and in the local galaxies as candidates for ULXs (Krolik, McKee, & Tarter 1981; Krolik & Kallman 1984; Krolik 2004; Ricotti & Ostriker 2004; Ricotti, Ostriker, & Gnedin 2005; Ricotti 2007; Strohmayer & Mushotzky 2009), and SMBHs in merging galaxies. Both radiation feedback and BH motion are expected to reduce the accretion rate with respect to the Bondi rate, but it is unknown what is the combined effect of these two processes. To the best of our knowledge, the present study is the first to consider radiation feedback effects on moving BHs.

This paper is organized as follows. In Section 2, we introduce basic definitions used throughout this series of papers and describe the numerical simulations. In Sections 3 and 4, we show our simulation results and the analytical model describing the set of simulations respectively. Finally, we summarize and discuss the implications of our work in Section 5.

2. BASIC DEFINITIONS AND RADIATION-HYDRODYNAMIC SIMULATIONS

For the sake of consistency with the previous papers of this series, we define the dimensionless accretion rate $\lambda_{\text{rad}} \equiv \dot{M}/\dot{M}_B$, where \dot{M}_B is the Bondi accretion rate for isothermal gas ($\gamma = 1$). In Paper II we found that the mean accretion rate for a stationary BHs regulated by radiation feedback is

$$\langle \dot{M} \rangle = \min (1\% T_{\infty,4}^{5/2} \dot{M}_B, \eta^{-1} \dot{M}_{\text{Edd}}), \quad (2)$$

where we have defined $T_{\infty,n} \equiv T_{\infty}/(10^n \text{ K})$. Equation (2) is valid for density $n_{\text{H},\infty} \gtrsim 10^5 M_2^{-1} \text{ cm}^{-3}$ where a similar definition $M_n \equiv M_{\text{bh}}/(10^n M_{\odot})$ is made. Instead, if $n_{\text{H},\infty} \lesssim 10^5 M_2^{-1} \text{ cm}^{-3}$, the dimensionless accretion rate in the sub-Eddington regime shows a dependency with the density $\langle \lambda_{\text{rad}} \rangle = 1\% T_{\infty,4}^{5/2} n_5^{1/2}$, where again we define $n_m \equiv n_{\text{H},\infty}/10^m \text{ cm}^{-3}$. The Eddington luminosity and accretion rates are defined as $L_{\text{Edd}} = 4\pi G M_{\text{bh}} m_p c \sigma_T^{-1} = (3.3 \times 10^6 L_{\odot}) M_2$, and $\dot{M}_{\text{Edd}} \equiv L_{\text{Edd}} c^{-2}$, respectively. Note that we have adopted a definition of \dot{M}_{Edd} independent of the radiative efficiency η , thus for Eddington limited accretion the

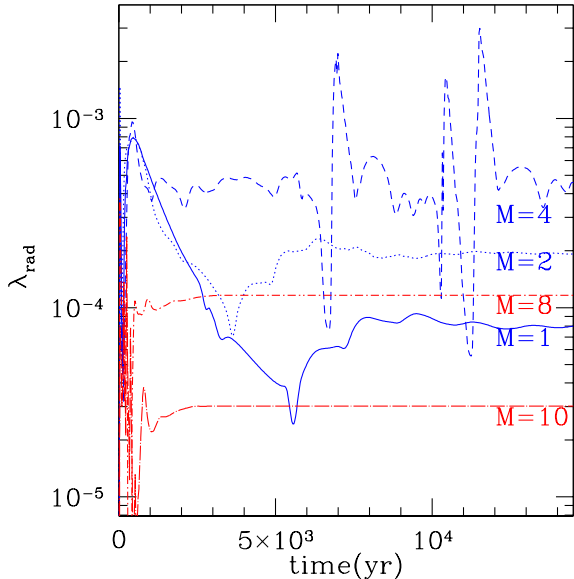


FIG. 1.— Accretion rate in units of the Bondi rate as a function of time for simulations with $M_{\text{bh}} = 100 M_{\odot}$, $n_{\text{H},\infty} = 10^3 \text{ cm}^{-3}$, and $T_{\infty} = 10^4 \text{ K}$. The lines show simulations for BH moving at Mach numbers $\mathcal{M} = 1, 2, 4, 8,$ and 10 (see labels under each line). The early phase in all the simulations shows oscillatory behavior of the accretion rate due to non-equilibrium initial conditions. However, in most simulations the accretion rate quickly reaches a steady state. The average accretion rate increases with increasing Mach number for Mach numbers from 1 to 4 and decreases for larger Mach numbers. Quasi-periodic bursts of accretion are seen in the simulation with $\mathcal{M} = 4$.

accretion rate in units of \dot{M}_{Edd} is $\dot{m} = 1/\eta > 1$.

The numerical method used in this paper is the same as in Papers I and II. We run a set of 2D radiation-hydrodynamic simulations using a modified parallel version of the non-relativistic hydrodynamics code ZEUS-MP (Stone & Norman 1992; Hayes et al. 2006) with our photon-conserving UV and X-ray one-dimensional radiative transfer equation solver (Ricotti et al. 2001; Whalen & Norman 2006). We include photo heating, photo ionization, and chemistry of H/He in multi-frequency are manifested in the code to see how high-energy UV and X-ray photons regulate gas accretion onto moving BHs. Radiation pressure both on electrons and H I is calculated to simulate the effect of momentum transfer from ionizing photons to gas. See Paper I and Paper II for detailed description.

Axis-symmetric geometry with respect to the azimuthal angle (ϕ) is applied to all simulations. We use logarithmically spaced grid in the radial direction (r), and evenly spaced grid in the polar angle direction ($0 \leq \theta \leq \pi$), with BH centered at the origin $r = 0$. Axis-symmetric configuration is necessary to simulate BHs in motion relative to ambient gas which is assumed to be moving parallel to the polar axes. In the radial direction we apply flow-in boundary conditions at the outer boundary for the first half of the polar angle ($0 \leq \theta \leq 0.5\pi$) and flow-out boundary conditions for the second half ($0.5\pi < \theta \leq \pi$). At the inner boundary, in the radial direction, we apply flow-out boundary condition for the entire polar angle. Reflective boundary conditions are applied along the polar axis $\theta = 0$ and $\theta = \pi$ to satisfy the axis-symmetric configuration.

We assume uniform density and constant velocity for the initial conditions. For the supersonic cases ($\mathcal{M} > 1$), we start the simulations with an assumption of fixed accretion

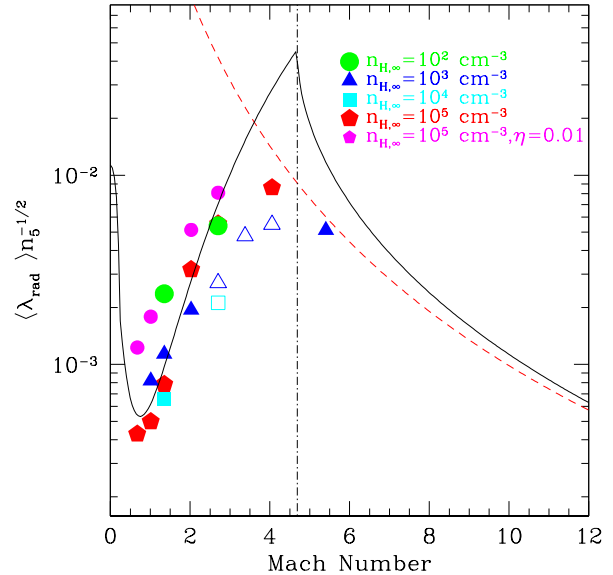


FIG. 2.— Mean accretion rate in units of the Bondi rate $\langle \lambda_{\text{rad}} \rangle$ as a function of BH Mach number. Classical Hoyle–Lyttleton accretion predicts a monotonic decrease of accretion rate as $\langle \lambda_{\text{rad}} \rangle \propto (1 + \mathcal{M}^2)^{-3/2}$ (dashed line). However our simulations (solid and open symbols) show that $\langle \lambda_{\text{rad}} \rangle$ decreases with \mathcal{M} for subsonic velocities, has a minimum at $\mathcal{M} \sim 1$, increases for $1 < \mathcal{M} \lesssim \mathcal{M}_R$, and decreases again for $\mathcal{M} > \mathcal{M}_R$. The solid line shows our model based on D -type I-front jump conditions preceded by an isothermal bow-shock forming in the upstream direction for $\mathcal{M} < \mathcal{M}_R$ and a transition to R -type I-front for Mach numbers larger than \mathcal{M}_R (shown by the dot-dashed line). The Y -axis shows $\langle \lambda_{\text{rad}} \rangle / n_{\text{H},\infty}^{1/2}$ because simulations with ambient densities $n_{\text{H},\infty} < 10^5 \text{ cm}^{-3}$ have $\langle \lambda_{\text{rad}} \rangle \propto n_{\text{H},\infty}^{1/2}$, in agreement with previous results for non-moving BHs (see Paper I). Solid symbols show simulations that reach a steady-state solution, while open symbols indicate simulations that present oscillatory behavior of the accretion rate due to instabilities of the thin-shell downstream of the bow shock.

rate ($\langle \lambda_{\text{rad}} \rangle = 0.001$) to reduce the effect of oscillation observed at early phases of the simulations. For our reference simulations, we select a fiducial value of the radiative efficiency $\eta = 0.1$, typical for thin disk models (Shakura & Sunyaev 1973), BH mass $M_{\text{bh}} = 100 M_{\odot}$, and the temperature of the ambient gas $T_{\infty} = 10^4 \text{ K}$. We explore a range of Mach numbers up to $\mathcal{M} = 10$, and gas densities $n_{\text{H},\infty} = 10^2$ – 10^5 cm^{-3} .

3. NUMERICAL RESULTS

3.1. Accretion Rate as a Function of Mach Number

The classical Bondi–Hoyle–Lyttleton accretion predicts a monotonic decrease of accretion rate with increasing velocity of the BH with respect to the ambient gas as in Equation (1). However, our simulations of moving BHs with radiative feedback show a very different dependence of accretion rate as a function of the Mach number.

Figure 1 shows the time evolution of accretion rate for different Mach numbers $\mathcal{M} = 1, 2, 4, 8,$ and 10 for gas density $n_{\text{H},\infty} = 10^3 \text{ cm}^{-3}$. Most simulations, except the one with $\mathcal{M} = 4$, show steady accretion rates after an initial transient phase that is the result of out-of-equilibrium initial conditions. The time duration of the transient phase is proportional to the crossing timescale τ_{cr} , and thus inversely proportional to the Mach number. The mean dimensionless accretion rate $\langle \lambda_{\text{rad}} \rangle$ (in units of the Bondi rate) is measured when the accretion reaches a steady state while for the non-steady cases, such as

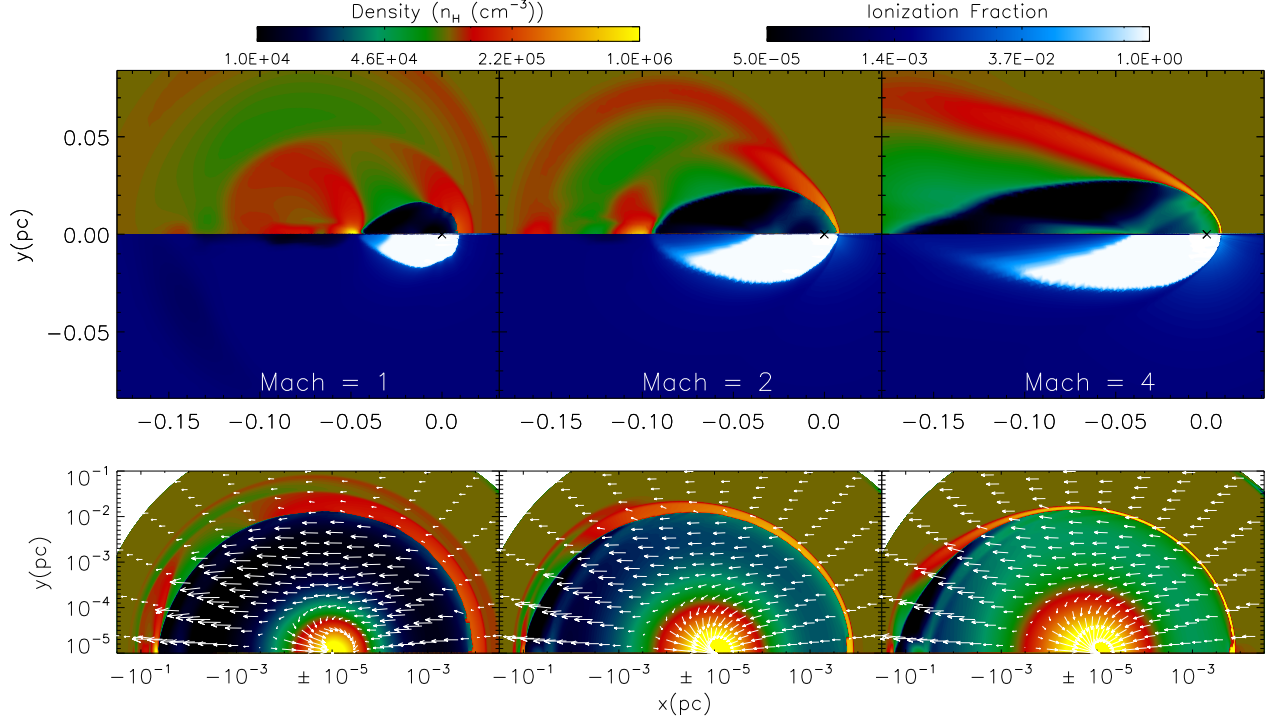


FIG. 3.— Top: density (top half of the panel) and ionization fraction (bottom half of the panel) for simulations of a BH of mass $M_{\text{bh}} = 100 M_{\odot}$, gas density $n_{\text{H},\infty} = 10^5 \text{ cm}^{-3}$, and temperature $T_{\infty} = 10^4 \text{ K}$ moving at $\mathcal{M} = 1, 2,$ and 4 (from left to right). Each panel shows a large-scale view of the cometary-shaped H II region and the dense shell in the upstream direction for simulation with different Mach numbers. The size of the Strömgen sphere in the downstream direction increases roughly linearly with increasing Mach number but remains roughly constant as a function of Mach number in the upstream direction. With increasing Mach number, the density of the shell in the upstream direction increases ($(n_{\text{H,sh}}/n_{\text{H},\infty}) \propto \mathcal{M}^2$) and the density behind the dense shell also increases $n_{\text{H,in}}/n_{\text{H},\infty} \propto \mathcal{M}^2$ for $1 < \mathcal{M} < \mathcal{M}_R$. Bottom: the same simulations as in the top panel but showing the gas density field and gas velocity vectors adopting logarithmic scale in the radial direction to emphasize the gas flow at small scales.

$\mathcal{M} = 4$, we calculate the time-averaged accretion rate. As found in Paper I, at low gas densities, i.e., $n_{\text{H},\infty} \lesssim 10^5 \text{ cm}^{-3}$ for simulations with $M_{\text{bh}} = 100 M_{\odot}$, $\langle \lambda_{\text{rad}} \rangle$ is proportional to square root of density ($\langle \lambda_{\text{rad}} \rangle \propto n_{\text{H},\infty}^{1/2}$). Figure 2 shows that after correcting $\langle \lambda_{\text{rad}} \rangle$ for the aforementioned density dependence also found for stationary BH, the same functional form for the accretion rate fits all simulations with different gas densities (large symbols for $\eta = 0.1$ and gas densities $n_{\text{H},\infty} = 10^2\text{--}10^5 \text{ cm}^{-3}$) and radiative efficiencies (small pentagons for a simulation with $\eta = 0.01$ and $n_{\text{H},\infty} = 10^5 \text{ cm}^{-3}$). Open symbols indicate simulations that show non-steady accretion rate due to instabilities of the dense post-shock layer forming in the upstream direction (see Section 4.3).

The quasi-periodic oscillations of the accretion rate found in Paper I and Paper II for stationary BHs are still observed in simulations with low Mach numbers $\mathcal{M} \lesssim 0.5$, which maintain the main characteristics of spherically symmetric accretion discussed in Paper I and Paper II. This implies that introducing small systematic subsonic velocity to spherically symmetric accretion does not significantly alter the oscillatory behavior of the accretion. However, the average accretion rate $\langle \lambda_{\text{rad}} \rangle$ decreases steeply as a function of Mach number in this Mach number range, and $\langle \lambda_{\text{rad}} \rangle$ at $\mathcal{M} \sim 1$ is roughly one order of magnitude smaller than for non-moving BHs (including radiation feedback), and three orders of magnitude smaller compared to stationary BHs with no radiative feedback, when all the other parameters are held constant. This decrease of the accretion rate with increasing velocity found for subsonic BH velocities is only *qualitatively* similar to Bondi–Hoyle–

Lyttleton accretion, but does not have the same scaling with BH velocity.

The spherically symmetric accretion model fails for supersonic BH motion ($\mathcal{M} \gtrsim 1$). The shape of the H II region makes a transition to a well-defined axis-symmetric geometry, elongated along the direction of the gas flow in the downstream direction, while a bow-shaped dense shell develops in front of the H II region in the upstream direction, significantly affecting the velocity field of the gas inflow. In most simulations, steady-state accretion is achieved for supersonic BH motion, since gas is continuously supplied to the BH without interruption.

Interestingly, as the BH motion becomes supersonic and a bow-shock and dense shell form, $\langle \lambda_{\text{rad}} \rangle$ increases as a function of Mach number. This is clearly at odds with the results expected from the classical Bondi–Hoyle–Lyttleton model. A Mach number of $\mathcal{M} \sim 1$ is roughly the turning point where $\langle \lambda_{\text{rad}} \rangle$ has a minimum, while there is a maximum value of the Mach number $\mathcal{M} = \mathcal{M}_R$ ($\mathcal{M}_R \sim 4$ for $T_{\infty} = 10^4 \text{ K}$), at which $\langle \lambda_{\text{rad}} \rangle$ reaches a maximum value, before starting to decrease with increasing BH velocity. An instability of the dense shell that leads to bursts of accretion rate is observed in some simulations in this Mach number range. This result will be discussed in Section 4.3. At higher Mach numbers ($\mathcal{M} > \mathcal{M}_R$), a steady-state solution is achieved once again since the dense shell does not form due to the high velocity of the gas inflow (as shown in Section 4.1, the I-front transitions from *D*-type to *R*-type). For $\mathcal{M} > \mathcal{M}_R$, $\langle \lambda_{\text{rad}} \rangle$ decreases monotonically as a function of Mach number and converges to the Bondi–Hoyle–Lyttleton solution (with no radiative feed-

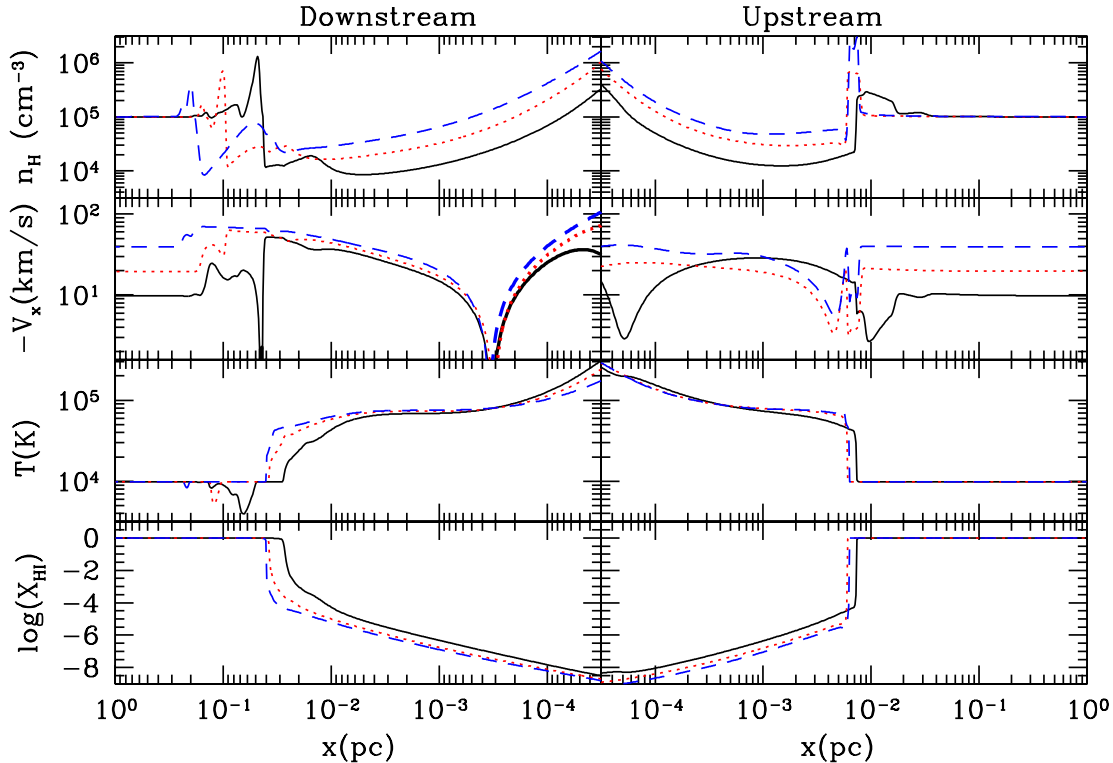


FIG. 4.— Density, velocity, temperature, and H I abundance (from top to bottom) profiles along X -axis (axis of symmetry) for the simulations shown in Figure 3 for $\mathcal{M} = 1$ (solid lines), 2 (dotted), and 4 (dashed). The left panels (note that small scales are on the right side) show profiles in the downstream direction while the right panels show upstream profiles.

back) shown as a dashed line in Figure 2. In this high velocity regime, the I-front becomes R -type and the gas flow is weakly affected by radiative feedback.

3.2. Structure of the Gas Flow and H II Region

For Mach numbers $1 < \mathcal{M} < \mathcal{M}_R$, a dense bow shock forms in front of the H II region in the upstream direction, followed by a D -type I-front (see Figure 3). Most of the gas inflow propagates through the bow shock without changing direction, while a small fraction of the gas inflow in the outer parts of the bow shock is re-directed farther from the axis of symmetry. The formation of a bow shock in the upstream direction changes the gas density and velocity behind the shock, while the gas temperature remains relatively unaffected (isothermal shock). Note that the H II region has a cometary shape, with overall length increasing linearly with increasing Mach number. The size of the H II region in the upstream direction is not sensitive to the Mach number, while in the downstream direction the length of the ionized tail shows a linear relationship with the Mach number as shown in Figure 3. The upper panels in Figure 3 show the changes in the density structure and the H II region shape for $\mathcal{M} = 1, 2$, and 4, respectively. The lower panels show the vector fields over the gas density for each simulation. In the bottom panels, we use a logarithmic scale for the radial direction to better show the motion of gas in the vicinity of the BH. The location Bondi radius calculated for the gas temperature inside the H II region is close to, but within the location of the I-front. We will see in the next section that this will allow us to derive simple analytical formulae for the accretion rate

using the Bondi formula for the gas inside the H II region and a model for the I-front.

For $\mathcal{M} = 1$, the size of the H II region in the downstream direction is roughly ~ 4 times its length in the upstream direction. The density structure in the downstream direction is very complex as shown in Figure 3. The re-directed gas streams form high-density regions and shocks. However, since most of the gas downstream of the BH is not accreted onto the BH, we will focus on understanding the upstream structures. The size of the H II region in the upstream direction will be discussed in greater detail in Section 5.

4. ANALYTIC MODELING

In this section we show that properties of the gas flow around the moving BH can be understood using a simple one-dimensional model for a standing I-front in the frame of reference moving with the BH. There are two regimes for the I-fronts: an R -type front and D -type front, determined by the BH velocity and density of the ambient medium. As in the previous papers we find that the accretion rate onto the BH can be estimated using the Bondi–Lyttleton formula for the gas inside the I-front, since the effective Bondi radius lays within the ionized region.

4.1. Transition from R -type to D -type I-front

In most simulations, we found that the gas flow reaches a steady-state solution. In these cases, the position of the I-front with respect to the BH is stationary, hence the I-front propagates with respect to the gas upstream with constant velocity v_{bh} . Although the geometry of the H II region and the

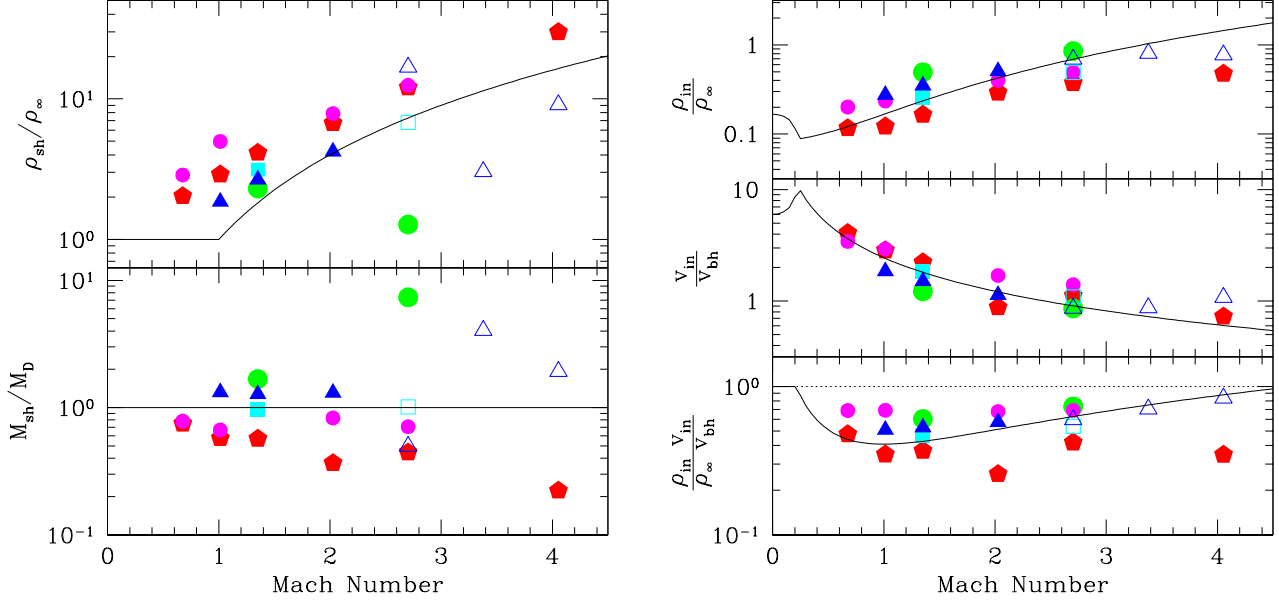


FIG. 5.— Left: density (top panel) and Mach number (bottom panel) of gas in the dense shell in the upstream direction in the simulations shown in Figure 2. The lines show the model predictions based on isothermal shock jump conditions ($\rho_{\text{sh}}/\rho_{\infty} \propto \mathcal{M}^2$) for the curved bow shock (see the text). Right: density, velocity and mass flux of gas inside the H II region in various simulations. The lines show the model predictions assuming D -type I-front (see the text). The symbols have the same meaning as in Figure 2.

bow shock are clearly not planar, we can approximate the flow as one-dimensional (parallel to the direction of motion of the BH) near the I-front location in the region around the axis of symmetry of the problem. But we will show that accounting for deviations from the planar symmetry is necessary to understand the simulations results.

Let us start by writing down the equations for the propagation of one-dimensional I-front through an homogeneous medium with density ρ_{∞} . The density ratio across the I-front can be estimated by solving the mass and momentum conservation conditions $\rho_{\text{in}}v_{\text{in}} = \rho_{\infty}v_{\text{bh}} = J\mu$, where J is radiation flux and $\mu = 1.27m_H$, assuming the helium becomes singly ionized in the front (Spitzer 1978):

$$\Delta_{\rho} \equiv \frac{\rho_{\text{in}}}{\rho_{\infty}} = \frac{(1 + \mathcal{M}^2) \pm \sqrt{(1 + \mathcal{M}^2)^2 - 4\mathcal{M}^2\Delta_T}}{2\Delta_T}. \quad (3)$$

Here, we have defined $\Delta_T \equiv T_{\text{in}}/T_{\infty} \geq 1$. Due to the condition for the density ratio in Equation (3) to have real positive values, the Mach number must be $\mathcal{M} \leq \mathcal{M}_D$, where D stands for *dense* gas, or $\mathcal{M} \geq \mathcal{M}_R$ where R refers to *rarefied* gas. D - and R -critical Mach numbers are respectively:

$$\mathcal{M}_D = \sqrt{\Delta_T} (1 - \sqrt{1 - 1/\Delta_T}) \xrightarrow{\Delta_T \gg 1} \frac{1}{2\sqrt{\Delta_T}}, \quad (4)$$

$$\mathcal{M}_R = \sqrt{\Delta_T} (1 + \sqrt{1 - 1/\Delta_T}) \xrightarrow{\Delta_T \gg 1} 2\sqrt{\Delta_T}. \quad (5)$$

Also, $\mathcal{M}_D\mathcal{M}_R = 1$, thus $\mathcal{M}_D \equiv \mathcal{M}_R^{-1}$. In terms of the BH velocity the critical velocities are:

$$v_D = c_{s,\text{in}} (1 - \sqrt{1 - 1/\Delta_T}) \xrightarrow{\Delta_T \gg 1} \frac{c_{s,\infty}^2}{2c_{s,\text{in}}}, \quad (6)$$

$$v_R = c_{s,\text{in}} (1 + \sqrt{1 - 1/\Delta_T}) \xrightarrow{\Delta_T \gg 1} 2c_{s,\text{in}}. \quad (7)$$

Only for the special case in which $\Delta_T \simeq 1$, we have $\mathcal{M}_D \simeq \mathcal{M}_R \simeq 1$ and a solution exists for any BH velocity. However,

for all physically motivated cases with $\Delta_T > 1$ a solution is not possible for BH velocities $v_D < v_{\text{bh}} < v_R$. In our simulations if $v_{\text{bh}} > v_R \sim 2c_{s,\text{in}}$ the analytical solution that reproduces the data is the one with the negative sign in Equation (3). This solution describes a weak R -type I-front, that has $\rho_{\text{in}} \sim \rho_{\infty}$ and supersonic motions of the gas both ahead and behind the I-front (in the frame of reference comoving with the BH).

If $v_D < c_{s,\infty}/2 < v_{\text{bh}} < v_R \sim 2c_{s,\text{in}}$ a solution is not possible. A shock front must precede the I-front, increasing the density and reducing the gas velocity below v_D (D -type solution). This is indeed observed in the simulations. For a D -type front, the density past the front is always lower than the density upstream. Figure 4 shows that the post-shock density and velocity are a function of the Mach number, while the temperature of the shell is always $T_{\text{sh}} \approx T_{\infty}$, i.e., the shock is isothermal ($\gamma = 1$). The ratio between the densities at infinity and behind the isothermal shock is

$$\frac{\rho_{\text{sh}}}{\rho_{\infty}} \simeq \mathcal{M}^2, \quad (8)$$

that is in good agreement with the simulation results (see Figure 5, left panel). However, for the calculation of the gas velocity in the shell our simplifying assumption of planar geometry fails. Assuming planar geometry, mass flux conservation in the direction of the BH motion implies $\rho_{\text{sh}}v_{\text{sh}} = \rho_{\infty}v_{\text{bh}}$. Thus, the Mach number in the shell $\mathcal{M}_{\text{sh}} \equiv v_{\text{sh}}/c_{s,\text{sh}}$ is $\mathcal{M}_{\text{sh}} = \mathcal{M}^{-1} < 1$. However, this assumption fails to reproduce the simulation results and is inconsistent with obtaining a D -type solution for the I-front. Hence, the model must assume (as verified in the simulations) that the gas velocity inside the shell has a non-zero tangential component. It follows that the component of the velocity along the direction of motion of the BH is reduced due to off-axis motions that divert some of the gas in the direction parallel to the bow shock. As illustrated in left panel in Figure 5, the simulations do not

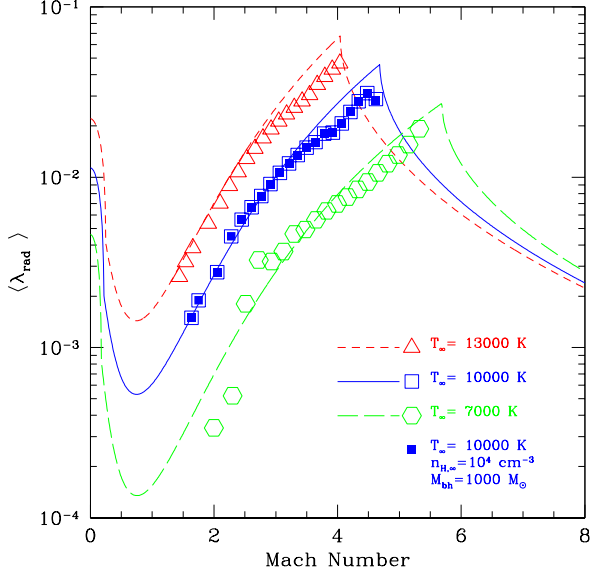


FIG. 6.— Accretion rates as a function of Mach number for “wind-tunnel” simulations with $M_{\text{bh}} = 100 M_\odot$, $n_{\text{H},\infty} = 10^5 \text{ cm}^{-3}$, and $\eta = 0.1$. Different lines and symbols show the model and simulations respectively for gas temperatures at infinity $T_\infty = 7,000 \text{ K}$ (long-dashed line, open hexagons), $10,000 \text{ K}$ (solid line, open squares), and $13,000 \text{ K}$ (short-dashed line, triangles). Solid squares show simulations with $T_\infty = 10,000 \text{ K}$ but BH mass 10 times higher ($M_{\text{bh}} = 1000 M_\odot$) and ambient gas density 10 times lower ($n_{\text{H},\infty} = 10^4 \text{ cm}^{-3}$) than the other runs in this figure. The accretion rates for the two simulations with $T_\infty = 10,000 \text{ K}$ (solid and open squares) are indistinguishable.

indicate a strong trend of \mathcal{M}_{sh} with \mathcal{M} :

$$\mathcal{M}_{\text{sh}} \sim \mathcal{A} \mathcal{M}_D, \text{ with } \mathcal{A} \lesssim 1, \quad (9)$$

implying that $v_{\text{sh}} \rho_{\text{sh}} / (\rho_\infty v_{\text{bh}}) = \mathcal{A} (\mathcal{M} / \mathcal{M}_R) < 1$. Note that in order to be consistent with our model, the data points for \mathcal{M}_{sh} are calculated from the simulation data by enforcing mass conservation across the I-front: $\mathcal{M}_{\text{sh}} = \rho_{\text{in}} v_{\text{in}} / (\rho_{\text{sh}} c_{\text{s,sh}})$. This ensures that the jump conditions across the I-front ignore the component of the velocity parallel to the bow shock.

As discussed above, across the I-front, the density ratio between the gas in the shell and in the H II region can be estimated by solving the mass and momentum conservation conditions:

$$\frac{\rho_{\text{in}}}{\rho_{\text{sh}}} = \frac{(1 + \mathcal{M}_{\text{sh}}^2) \pm \sqrt{(1 + \mathcal{M}_{\text{sh}}^2)^2 - 4\mathcal{M}_{\text{sh}}^2 \Delta_T}}{2\Delta_T} \quad (10)$$

$$\sim 2\mathcal{M}_D^2 \text{ for } \mathcal{A} \sim 1.$$

For Equation (10) to have real positive values, we must have $\mathcal{M}_{\text{sh}} \leq \mathcal{M}_D = \mathcal{M}_R^{-1}$ (D -type solution). Clearly, if $\mathcal{A} \leq 1$ (i.e. $\mathcal{M}_{\text{sh}} \leq \mathcal{M}_D$) a D -type solution is possible for any Mach number $\mathcal{M} < \mathcal{M}_R$. Note that a D -type solution would not be possible if we had assumed one-dimensional flow geometry for which $\mathcal{M}_{\text{sh}} = \mathcal{M}^{-1}$. One-dimensional flow assumption would give a D -type solution only for $\mathcal{M} > \mathcal{M}_R$, that is the regime in which we expect an R -type front, and is thus ruled out. In general, for $\mathcal{A}^2 < 1$ the D -type solution consistent with the simulations results is the one with the negative sign in Equation (10), which has the larger relative decrease in density across the front: $\rho_{\text{in}} / \rho_{\text{sh}} \sim \mathcal{A}^2 \mathcal{M}_D^2$. This solution describes a strong D -type front. By combining Equations (8)–

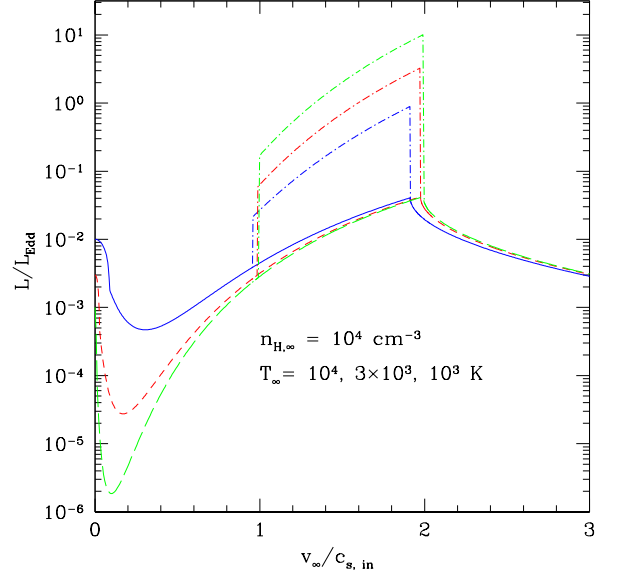


FIG. 7.— Accretion luminosity normalized by the Eddington rate as a function of the BH velocity v_{bh} in units of the sound speed inside the H II region for BH mass $M_{\text{bh}} = 100 M_\odot$, $n_{\text{H},\infty} = 10^4 \text{ cm}^{-3}$, and $\eta = 0.1$. Different line types are used for models with different temperatures: $T_\infty = 10^4$ (solid), 3×10^3 (short dashed), and 10^3 K (long dashed). Note that the accretion rates peak at $v_{\text{bh}} \sim 2c_{\text{s,in}}$ regardless of T_∞ . Dot-dashed lines for each temperature T_∞ show possible enhanced luminosities when the thin shell in front of the I-front becomes unstable producing periodic accretion bursts. Accretion of high-density gas from the broken dense shell remnants with density $\rho_{\text{sh}} \propto \mathcal{M}^2$ can increase the peak accretion rates by a factor \mathcal{M}^2 .

(10), we obtain

$$\Delta_\rho \equiv \frac{\rho_{\text{in}}}{\rho_\infty} = \frac{\rho_{\text{in}} \rho_{\text{sh}}}{\rho_{\text{sh}} \rho_\infty} \quad (11)$$

$$\approx \frac{\mathcal{M}^2}{2\Delta_T} \approx 2 \left(\frac{\mathcal{M}}{\mathcal{M}_R} \right)^2 \text{ for } \mathcal{A} \sim 1, \quad (12)$$

or $\Delta_\rho = \mathcal{A}^2 (\mathcal{M} / \mathcal{M}_R)^2$ for $\mathcal{A}^2 < 1$. The velocity ratio between the gas inside the H II region and the BH velocity is $v_{\text{in}} / v_{\text{bh}} = (\rho_{\text{sh}} / \rho_{\text{in}}) (\mathcal{M}_{\text{sh}} / \mathcal{M}) \approx \mathcal{M}_R / 2\mathcal{M}$ for $\mathcal{A} \sim 1$ or $v_{\text{in}} / v_{\text{bh}} = \mathcal{M}_R / \mathcal{A} \mathcal{M}$ for $\mathcal{A}^2 < 1$. In this regime (D -type I-front) the model predicts that the Mach number of the gas inside the H II region is a constant close to unity, as is indeed observed in all the simulations: $\mathcal{M}_{\text{in}} \approx (v_{\text{in}} / v_{\text{bh}}) (\mathcal{M} / \Delta_T^{1/2}) \approx 1$ for $\mathcal{A} \sim 1$ (or $\mathcal{M}_{\text{in}} = 2 / \mathcal{A}$ for $\mathcal{A}^2 < 1$).

The symbols in the upper left panel in Figure 5 show the ratio between the gas density at infinity and inside the dense shell as a function of \mathcal{M} for a set of simulations with different parameters (i.e., gas density and radiative efficiency as shown in the figure’s legend). Our model is shown as a solid line. The lower left panel shows the Mach number in the shell \mathcal{M}_{sh} in units of \mathcal{M}_D , as a function of \mathcal{M} for the same simulations. The right panels in Figure 5 show the density and velocity ratios between the gas at infinity and inside the H II region as a function of Mach number. We measure the gas density and velocity within the H II region where the density profiles have a minimum behind the I-front. As discussed above, for a plane parallel I-front and shock the mass flux of the gas is conserved: $\rho_{\text{in}} v_{\text{in}} / (\rho_\infty v_{\text{bh}}) = 1$. However, due to the formation of a bow shock when the I-front becomes D -type, the gas flow has a velocity compo-

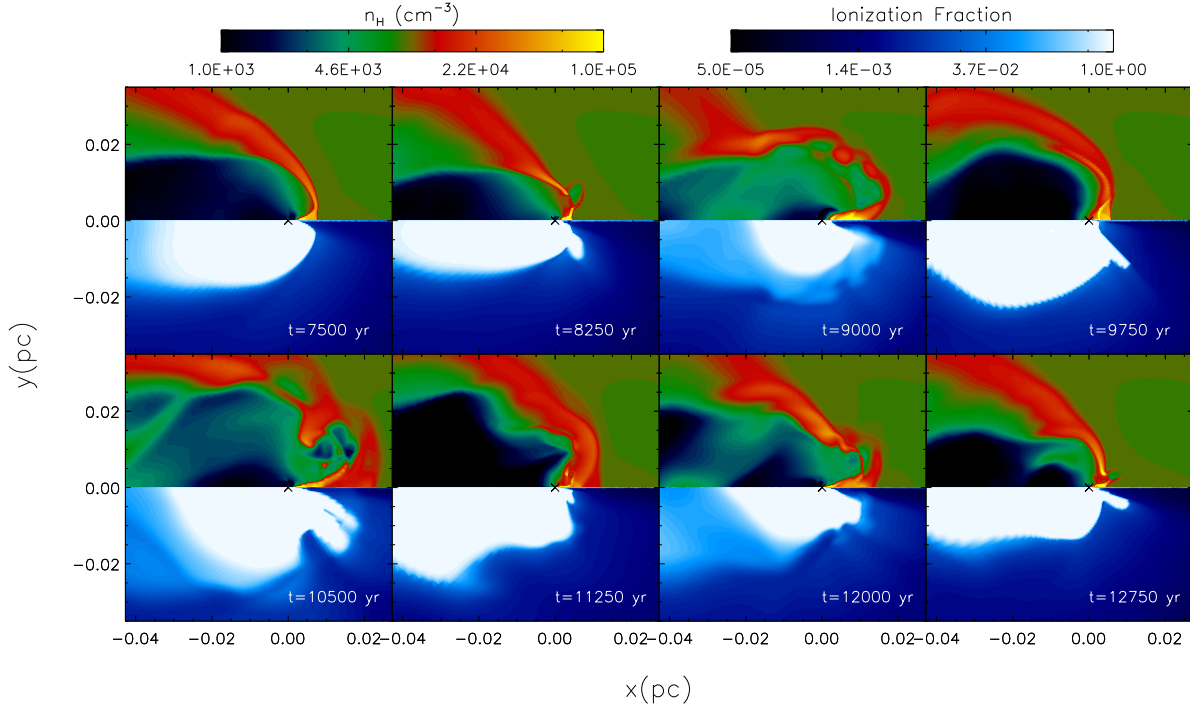


FIG. 8.— Snapshots showing the time evolution of the density (top half of the panels) and ionization fraction (bottom half of the panels) in a simulation of a BH of mass $M_{\text{bh}} = 100 M_{\odot}$, gas density 10^4 cm^{-3} , and temperature $T_{\infty} = 10^4 \text{ K}$ moving at $\mathcal{M} = 2.7$. The dense gas shell upstream of the bow shock forms and gets destroyed with a quasi-periodic behavior. When the dense shell breaks and falls onto the BH, the accretion rate shows peak luminosities which are much higher than the average depending on the density of the shell, and thus the Mach number \mathcal{M} .

nent perpendicular to the direction of the BH motion and $\rho_{\text{in}} v_{\text{in}} / (\rho_{\infty} v_{\text{bh}}) \approx \mathcal{M} / \mathcal{M}_R < 1$, in agreement with the simulation results shown in the right bottom panel of Figure 5. In our fiducial simulations with $T_{\infty} = 10^4 \text{ K}$, we have $\mathcal{M}_R \sim 4.7$ ($\Delta_T \simeq 6$ and $T_{\text{in}} = 6 \times 10^4 \text{ K}$). The simulation results confirm that a *D*-type I-front forms for $\mathcal{M} < \mathcal{M}_R$, while a transition to *R*-type occurs at $\mathcal{M} \sim \mathcal{M}_R$.

4.2. Accretion Rate

In this section, we describe a model that fits the gas accretion rates measured at the inner boundary (i.e., near the BH) in all our simulations. Since the effective Bondi radius calculated using the velocity and the sound speed inside the H II region is smaller than the radius of the I-front in the upstream direction, we can treat this problem as a “mini” Bondi accretion within the H II region. The mean accretion rate can be estimated using the Bondi–Hoyle–Lyttleton formula for gas inside the H II region: $\dot{M} \propto M_{\text{bh}}^2 \rho_{\text{in}} c_{\text{s,in}}^{-3} (1 + \mathcal{M}_{\text{in}}^2)^{-3/2}$. As in previous papers of this series, we define the dimensionless accretion rate in units of the Bondi rate $\dot{M}_B \propto M_{\text{bh}}^2 \rho_{\infty} c_{\text{s,\infty}}^{-3}$:

$$\langle \lambda_{\text{rad}} \rangle \equiv \frac{\dot{M}}{\dot{M}_B} = \frac{\rho_{\text{in}}}{\rho_{\infty}} \left(\frac{c_{\text{s,\infty}}}{c_{\text{s,in}}} \right)^3 \frac{1}{(1 + \mathcal{M}_{\text{in}}^2)^{3/2}} \quad (13)$$

$$= \frac{\Delta_{\rho}}{\Delta_T^{3/2}} \frac{1}{(1 + \mathcal{M}_{\text{in}}^2)^{3/2}}. \quad (14)$$

We have identified two regimes corresponding to the *D*-type and *R*-type I-front solutions. If $1 < \mathcal{M} \leq \mathcal{M}_R$, in the previous section we found $\Delta_{\rho} \approx 2(\mathcal{M}/\mathcal{M}_R)^2 = 2(v_{\text{bh}}/v_R)^2$, and $\mathcal{M}_{\text{in}} \approx 1$. This means that inside the H II region the density increases as the BH moves faster but the Mach number remains constant (approximately transonic). This model

explains in simple terms the increase in the accretion rate with increasing BH velocity observed in the simulations in this regime. If $\mathcal{M} > \mathcal{M}_R$, the shock front does not form and $\Delta_{\rho} \rightarrow 1$ (if $\mathcal{M} \gg \mathcal{M}_R$), while the Mach number is $\mathcal{M}_{\text{in}} \approx \mathcal{M}/\Delta_{\rho}/\Delta_T^{1/2}$. Hence, in dimensionless units:

$$\langle \lambda_{\text{rad}} \rangle \approx \begin{cases} (2\Delta_T)^{-5/2} \mathcal{M}^2 \approx \frac{2^{5/2}}{\mathcal{M}_R^3} \left(\frac{\mathcal{M}}{\mathcal{M}_R} \right)^2, & \text{if } \mathcal{M} \leq \mathcal{M}_R \\ \Delta_{\rho}^4 (\Delta_{\rho}^2 \Delta_T + \mathcal{M}^2)^{-3/2} \xrightarrow{\mathcal{M} \gg \mathcal{M}_R} [(\mathcal{M}_R/2)^2 + \mathcal{M}^2]^{-3/2}, & \text{if } \mathcal{M} > \mathcal{M}_R. \end{cases} \quad (15)$$

The solid line in Figure 2 shows our model for the accretion rate onto moving BHs. The model generally is a good fit to the simulation results, except the model slightly overestimates the accretion rate around the critical Mach number \mathcal{M}_R .

We run a complementary set of simulations to study more precisely the changes of the physical properties as a function of Mach number, since the simulations with constant velocities have a coarse sampling in velocity space and show an intrinsic scatter which is probably the result of out-of-equilibrium initial conditions. We start the simulation assuming sonic motion of the BH ($\mathcal{M} \sim 1$) and increase gradually the velocity of the gas inflow at the boundary. This type of “wind-tunnel” numerical experiments is useful to focus on the changes of physical properties as a function of velocity, while holding the other parameters fixed. The critical Mach number \mathcal{M}_R and the peak luminosity depend on the temperature ratio Δ_T as in Equation (5). Figure 6 shows the accretion rate as a function of Mach number for different gas temperatures at infinity $T_{\infty} = 7 \times 10^3, 10^4$, and $1.3 \times 10^4 \text{ K}$ for $M_{\text{bh}} = 100 M_{\odot}$, $n_{\text{H},\infty} = 10^5 \text{ cm}^{-3}$, and $\eta = 0.1$. Our

model is in good agreement with the simulation results as shown in Figure 6. The peak accretion rates and the critical Mach numbers in these cases are very close to the model predictions. However, the caveat is that the dense shell which initially forms at the beginning of the simulations does not change its location as the velocity of gas increases as observed in the simulations in which v_{bh} was held constant.

If we express the accretion rate as a function of the BH velocity in physical units, we find that the accretion rate is independent of the temperature of the ambient medium and peaks at about twice the sound speed inside the H II region: $v_{\text{bh}}^{\text{max}} = v_R \simeq 2c_{\text{s,in}}$ (see Figure 7). This is contrary to the case of a static BH (or moving at subsonic speed) for which $\langle \lambda_{\text{rad}} \rangle \propto T_{\infty}^{5/2}$ and hence the accretion rate $\dot{M} \propto T_{\infty}$ is proportional to the temperature of the ambient gas. The gas accretion rate for a moving BH is

$$\dot{M} \approx \frac{\rho_{\infty} (GM_{\text{bh}})^2}{c_{\text{s,in}}^3} \times \begin{cases} 0.7 \left(\frac{v_{\text{bh}}}{2c_{\text{s,in}}} \right)^2 & \text{if } c_{\text{s,\infty}} < v_{\text{bh}} \leq 2c_{\text{s,in}} \\ [1 + (v_{\text{bh}}/c_{\text{s,in}})^2]^{-3/2} & \text{if } v_{\text{bh}} \gg 2c_{\text{s,in}} \end{cases} \quad (16)$$

The velocity for peak accretion depends only on the sound speed inside the H II region and is $v_R = 50 \text{ km s}^{-1}$ for $T_{\text{in}} = 6 \times 10^4 \text{ K}$ ($c_{\text{s,in}} = 25 \text{ km s}^{-1}$). We find a mild dependence of T_{in} on the density of the ambient medium. As explored in more detail in Paper I, T_{in} depends on the hardness of the spectrum emitted by the BHs, the gas metallicity, and Compton cooling/heating.

Our model has a peak accretion rate of about 70% of the Bondi rate in a gas with temperature T_{in} and density ρ_{∞} , in good agreement with our “wind-tunnel” type simulations (however, as noted before, the simulations with constant BH Mach number produce smaller accretion rates at peak accretion: about a factor of five smaller than the model prediction for the peak value). Interestingly, in our model and simulations a BH moving at 20–50 km s^{-1} with respect to a gas with temperature $T_{\infty} \lesssim 10^4 \text{ K}$, has a faster growth rate and accretion luminosity than if it was at rest (or moving at subsonic speed). Figure 7 is an extrapolation of our results to lower temperature regime showing accretion rates as a function of BH velocity v_{bh} for gas temperatures $T_{\infty} = 10^4, 3 \times 10^3$, and 10^3 K . In all cases, if $T_{\infty} < 10^4 \text{ K}$, we find that the peak accretion rate at $v_{\text{bh}} \sim 2c_{\text{s,in}}$ is larger than the corresponding accretion rate onto a stationary BH. Clearly this is an important result because significant BH accretion is only possible when the BH is in a dense medium, for instance, a molecular cloud or the cold neutral medium in a galaxy, that generally have low temperatures. In addition, the colder the gas the smaller the BH velocity needs to be to achieve the supersonic speed that leads to significant increase of the BH accretion rate.

In the next section, we will discuss another important result: in the regime when the I-front is *D*-type, instabilities of the dense and thin shell behind the bow shock may lead to its fragmentation and hence produce periodic oscillations of the accretion rate and luminosity of the BH. This effect can further increase the peak accretion luminosity of the BH by roughly a factor \mathcal{M}^2 with respect to the mean values estimated above in Equation (16). For instance, the simulation with $\mathcal{M} \sim 3$, $n_{\text{H},\infty} = 10^4 \text{ cm}^{-3}$, and $T_{\infty} = 10^4 \text{ K}$ shows this instability and the peak accretion rate is roughly a factor of 10 larger than the mean.

4.3. Stability of Bow Shock and Periodic Oscillations of the Luminosity

As discussed in the previous section, the average accretion rate $\langle \lambda_{\text{rad}} \rangle$ increases with increasing Mach number if $1 < \mathcal{M} < \mathcal{M}_R$. For the lower values in this Mach number range, all simulations approach a steady-state accretion rate. Interestingly, as the Mach number approaches \mathcal{M}_R , the bow shock in simulations with ambient gas densities in the range $n_{\text{H},\infty} = 10^3\text{--}10^4 \text{ cm}^{-3}$, becomes unstable producing intermittent bursts of accretion due to a cyclic formation/destruction of a dense shell in the upstream direction (see Whalen & Norman 2011). Figure 8 shows time evolution of a simulation with $M_{\text{bh}} = 100 M_{\odot}$, gas density $n_{\text{H},\infty} = 10^4 \text{ cm}^{-3}$, temperature $T_{\infty} = 10^4 \text{ K}$, and Mach number $\mathcal{M} = 2.7$. As seen in Figure 3, the ionizing radiation creates a “cometary-shaped” H II region around the BH. In the early stages of the simulation, the gas flow remains relatively steady. However, with time some instabilities start growing leading to the fragmentation of the shell. As a result, the ionizing radiation and the hot gas inside the H II region are no longer contained by the dense shell downstream of the bow shock and an explosion takes place. Fragments from the broken dense shell fall onto the BH significantly increasing the accretion rate, thus creating more ionizing photons that blow out further the thinner parts of the shell. However, after a time delay from the burst roughly estimated as the H II region sound crossing time, the dense shell re-forms, resetting the initial conditions for the next burst cycle.

Since the dense shell is located outside the inner Bondi radius, the gravitational acceleration on the shell is relatively small and hence the time scale for Rayleigh–Taylor instability is long. In addition the radiation has a stabilizing effect as it tends to smooth out the growth of linear perturbations on small scales, that have the faster growth rate. However, when $v_{\text{bh}} \gtrsim c_{\text{s,in}}$ (i.e., $\mathcal{M} \sim \mathcal{M}_R/2$) the ram pressure becomes comparable to the thermal pressure inside the H II region and the I-front is pushed closer to the BH. In this case the increased gravitational acceleration on the shell and the increased sharpness of the pressure gradient seem to trigger the growth of instabilities. Also the column density of dense shell is roughly constant as a function of the BH velocity, hence because $\rho_{\text{sh}} \propto \mathcal{M}^2$ the thickness of the dense shell is $\propto \mathcal{M}^{-2}$. A thin shell is well known to be unstable (Vishniac 1994; Whalen & Norman 2008b,a).

As shown in Figure 5, in simulations at intermediate densities ($n_{\text{H},\infty} = 10^3\text{--}10^4 \text{ cm}^{-3}$) the Mach number in the dense shell is close but slightly larger than \mathcal{M}_D while for higher densities (10^5 cm^{-3}) is always less than \mathcal{M}_D . This implies that *D*-type solution for 10^5 cm^{-3} exists for all \mathcal{M} since $\mathcal{M}_{\text{sh}} < \mathcal{M}_D$ while a transition between *D*- and *R*-type is expected for $n_{\text{H},\infty} = 10^3\text{--}10^4 \text{ cm}^{-3}$. As shown in Figure 9, for simulations with $n_{\text{H},\infty} = 10^3 \text{ cm}^{-3}$ the interval between the bursts of accretion is fairly constant $\Delta t \sim 3000$ years.

In Paper I and Paper II we found a linear relationship between the average size of the Strömgren spheres $\langle R_s \rangle$ and the period between oscillations for stationary BHs, which is of a few 10^3 years for $M_{\text{bh}} = 100 M_{\odot}$ and $\eta = 0.1$. We have shown that this time scale is proportional to the sound crossing time of the H II region and have provided analytical relationships for the period. The same argument can be applied for interpreting the period between intermittent bursts for moving BHs and in the next section we provide a model that describes the size and shape of the H II region around

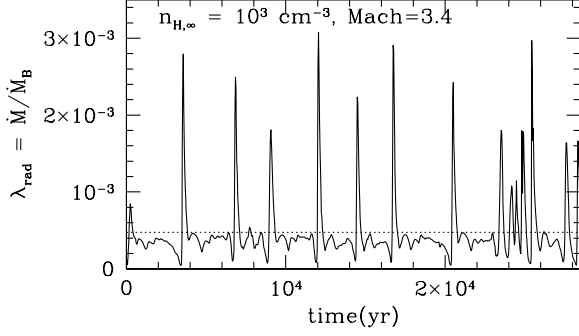


FIG. 9.— Accretion rate in units of the Bondi rate as a function of time in a simulation of a BH with mass $M_{\text{bh}} = 100 M_{\odot}$, gas density 10^3 cm^{-3} , and temperature $T_{\infty} = 10^4 \text{ K}$ moving at $\mathcal{M} = 3.4$. In this simulation, the dense gas shell upstream of the bow shock is unstable but after its fragmentation it re-forms on a timescale comparable to the H II region sound crossing time. When the dense shell breaks and falls onto the BH, the accretion rate shows peak luminosities which are an order of magnitude higher than the average (shown as dotted line).

moving BHs.

4.4. Size of H II Region in the Up/Downstream

The gas inflow in the direction of the polar axis $\theta = 0$ (upstream) and $\theta = \pi$ (downstream) can be approximated by a one-dimensional flow with the H II region being supplied with neutral gas with constant velocity v_{bh} . The total number of ionizing photons emitted by the BH must equal the number of hydrogen recombinations inside a radius $\langle R_s \rangle$ in addition to the flow through the I-front of neutral gas of density n and velocity v_{bh} :

$$N_{\text{ion}} = \frac{4\pi}{3} \langle R_s \rangle_{\theta}^3 \alpha_{\text{rec}} n_e^2 + 4\pi \langle R_s \rangle_{\theta}^2 n v_{\text{bh}} \cos(\theta), \quad (17)$$

where N_{ion} is the number of emitted ionizing photons, being directly related to the luminosity of the BHs (which is a function of Mach number). When the magnitudes of the two terms on the right side of Equation (17) are compared, at $\theta = 0$ the first term is dominant over the second term due to the BH motion. The electron number density inside the H II region for $1 < \mathcal{M} < \mathcal{M}_R$ is

$$n_e \sim x_e n_{\text{H,in}} = \frac{\mathcal{M}^2}{(2\Delta T)^{5/2}} n_{\text{H},\infty}. \quad (18)$$

Since $\langle \lambda_{\text{rad}} \rangle \propto n_{\text{H},\infty}^{1/2}$ (for $n_{\text{H},\infty} \lesssim 10^5 \text{ cm}^{-3}$ and $M_{\text{bh}} = 100 M_{\odot}$), the average size of the H II region in the upstream direction is

$$\langle R_s \rangle_{\theta=0} \propto \eta^{1/3} n_{\text{H},\infty}^{-1/6}. \quad (19)$$

Figure 10 shows the size of H II region at $\theta = 0$ as a function of Mach number for simulations with various densities ($n_{\text{H},\infty} = 10^2\text{--}10^5 \text{ cm}^{-3}$) and radiative efficiencies ($\eta = 0.1, 0.01$). The model is a good fit to the simulation results.

We model the size of the H II region in the downstream direction in a similar manner. In the downstream direction $\theta = \pi$ the second term on the right-hand side of Equation (17) dominates over the first term:

$$N_{\text{ion}} \simeq 4\pi \langle R_s \rangle_{\theta=\pi}^2 n_{\text{H,in}} v_{\text{bh}}, \quad (20)$$

where $n_{\text{H,in}}$ can be calculated simply using pressure equilibrium condition $n_{\text{H,in}} = n_{\text{H},\infty} \Delta T^{-1}$. The size of the H II region

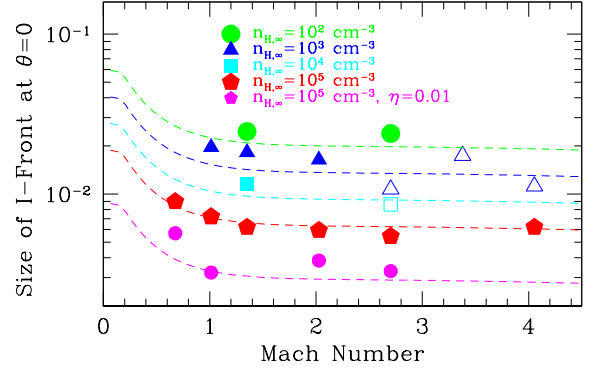


FIG. 10.— Size of H II region in the upstream direction ($\theta = 0$) $\langle R_s \rangle_{\theta=0}$ as a function of \mathcal{M} . Simulation results (symbols) show a good match with the model (lines). The symbols have the same meaning as in Figure 2. Since the recombination timescale τ_{rec} within the H II region is shorter than the H II region crossing time, $\langle R_s \rangle_{\theta=0}$ is not sensitive to the velocity of the flow. Also, $\langle R_s \rangle_{\theta=0}$ is very not sensitive to the density of the ambient medium since $\langle R_s \rangle_{\theta=0} \propto n_{\text{H},\infty}^{-1/6}$.

in the downstream direction for $1 < \mathcal{M} < \mathcal{M}_R$ is

$$\langle R_s \rangle_{\theta=\pi} \propto \eta^{1/2} n_{\text{H},\infty}^{1/4} (1 + \mathcal{M}^2)^{1/2}, \quad (21)$$

where $\langle R_s \rangle_{\theta=\pi}$ is approximately proportional to the Mach number. Figure 11 shows that the model reproduces the length of the tail of the H II region in the downstream direction in simulations for $n_{\text{H},\infty} = 10^5 \text{ cm}^{-3}$. The length of the H II region at $\theta = \pi$ is shorter than the model prediction because of the gravitational focusing of the gas by the BH that increases the gas density on the axis of symmetry behind the BH.

5. SUMMARY AND DISCUSSION

In this third paper of a series on radiation-regulated accretion onto BHs, we have focused on the effect of the BH motion relative to the surrounding gas, i.e., the Hoyle–Lyttleton problem modified by the effects that photo heating and radiation pressure from the radiation emitted near the BH have on the accretion flow. As in previous papers of this series, we have used radiation-hydrodynamic simulations to explore a large parameter space of initial conditions to inform us on how to formulate an analytical model that reproduces the simulation results. The followings are our key findings.

- The quasi-periodic oscillation of the accretion rate observed in simulations of non-moving BHs is only observed for subsonic motions of the BH, while the accretion rate becomes steady at supersonic velocities (in most cases).
- In the supersonic regime, we observe an axis-symmetric gas flow and a “cometary-shaped” H II region with tail length proportional to the BH velocity v_{bh} . For BH velocities $c_{s,\infty} < v_{\text{bh}} < v_R \approx 50 \text{ km s}^{-1}$ the ionization front becomes D -type: a bow shock and a dense shell develop in front of the H II region in the upstream direction. For $v_{\text{bh}} > v_R$ the bow shock disappears and the I-front becomes R -type.
- For subsonic motion of the BH we find that the accretion rate onto the BH decreases with increasing BH velocity. However, contrary to naive expectations, the accretion rate increases with increasing BH velocity in

the regime $c_{s,\infty} < v_{\text{bh}} < 50 \text{ km s}^{-1}$, when the I-front is D -type. The accretion rate peaks at BH velocity $v_{\text{bh}} \approx 50 \text{ km s}^{-1}$ before it starts decreasing with increasing BH velocity, converging to the well-known Hoyle–Lyttleton solution without radiation feedback.

- Based on the simulation results, we formulate a simple analytical model of the problem based on modeling the jump conditions across the I-front. The transition of the I-front from R -type to D -type happens at $v_{\text{bh}} = 2c_{s,\text{in}}$, where $c_{s,\text{in}}$ is the sound speed inside the H II region. An isothermal jump conditions for the bow shock reproduce fairly well the gas flow properties in simulations with ambient gas density $n_{\text{H},\infty} \gtrsim 10^2 \text{ cm}^{-3}$. Because the inner Bondi radius (for the gas inside the H II region) is comparable but smaller than the I-front radius, the accretion rate is well reproduced in our analytical model assuming Bondi-type accretion from the ionized gas downstream of the bow shock. The BH moves subsonically or transonically with respect to the gas downstream of the bow-shock. In this regime, the accretion rate increases with BH velocity because the density of the ionized gas inside the H II region increases with increasing velocity reaching $n_{\text{H}} \sim n_{\text{H},\infty}$ at $v_{\text{bh}} = 2c_{s,\text{in}}$.
- Simulations of BH accreting from a high-density medium ($n_{\text{H},\infty} = 10^5 \text{ cm}^{-3}$) show steady accretion rate for all Mach numbers. However, at intermediate densities ($n_{\text{H},\infty} = 10^3\text{--}10^4 \text{ cm}^{-3}$) we find intermittent bursts of accretion rate in the Mach number range $2.5 \lesssim \mathcal{M} \lesssim \mathcal{M}_R$. The oscillatory behavior of accretion rate is due to the development of instabilities in the thin shell in the upstream direction that cause its cyclic fragmentation and re-formation. In lower density regime, $n_{\text{H},\infty} \lesssim 10^2 \text{ cm}^{-3}$, the post-shock density is lower than expected assuming isothermal shock jump conditions; as a result the dense shell is thicker and less prone to instabilities. For $v_{\text{bh}} > v_R$ the dense shell never forms, providing steady accretion rates.
- Contrary to the case of radiation-regulated accretion onto non-moving BHs in which $\dot{M} \propto T_\infty^{5/2} \dot{M}_B \propto T_\infty$ (see Papers I and II), the accretion rate onto supersonic BHs is independent of the temperature of the ambient medium (see Equation (16)). It follows that if $T_\infty < 10^4 \text{ K}$ the accretion rate onto a BH moving with velocity $v_{\text{bh}} \approx 50 \text{ km s}^{-1}$ is about $5(10^4 \text{ K}/T_\infty)$ times larger than the accretion rate at $v_{\text{bh}} = 0$. Hence, the growth rate and the mean accretion luminosity of BHs moving supersonically can be significantly larger than that of non-moving BHs with the same mass and accreting from the same medium.

Our simulations are 2D, having assumed rotational symmetry around the axis defined by the BH motion and a spherically symmetric radiation field emitted near the BH. Below we discuss how our results and conclusions might be sensitive to the inclusion of the extra degree of freedom in more realistic three-dimensional simulations and different assumptions on the feedback mechanism.

It is well known that Hoyle–Lyttleton accretion without radiation feedback is prone to side to side “flip-flop” instability (e.g., Matsuda et al. 1987; Blondin & Pope 2009; Blondin & Raymer 2012) that cannot be captured in our axis-symmetric

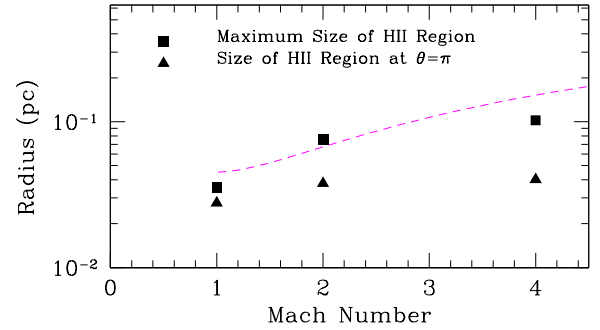


FIG. 11.— Size of H II region in the downstream direction as a function of \mathcal{M} . Maximum size of H II region and $\langle R_s \rangle_{\theta=\pi}$ are shown as squares and triangles, respectively. Our model shown as a dashed line approximately reproduces the maximum size of the H II region in the downstream direction (that has an offset from the axis of symmetry). The size of the H II region in the direction $\theta = \pi$ is smaller than the maximum size of the H II region due to gravitational focusing of gas by the BH that enhances the gas density along the axis (at $\theta = \pi$).

simulations. This instability breaks the axial symmetry of the flow downstream the BH where the gas, gravitationally focused by the BHs, is shocked and accreted. The resulting accretion of angular momentum produces the formation of temporary accretion disks spinning in alternating directions, with a burst of mass accretion when the direction of rotation is flipped. This non-axisymmetric instability has been seen in numerous hydrodynamic simulations of 2D planar accretion (Matsuda et al. 1991; Zarinelli et al. 1995; Benensohn et al. 1997; Shima et al. 1998; Pogorelov et al. 2000) but it has not been unambiguously identified in three-dimensional simulations (Ruffert 1999), possibly due to insufficient spatial resolution. In our simulations, radiation feedback may stabilize this instability for the cases, shown in Figure 3, when a stable bow-shock forms upstream of the BH. In this regime, the post-shock gas is transonic and the flow is better described by Bondi-type accretion than Hoyle–Lyttleton. For this reason, and because of the stabilizing effect of radiative heating (Blondin et al. 1990), the flip-flop instability may not be important in Hoyle–Lyttleton accretion when radiation feedback is included.

An extra spatial degree of freedom is likely to play a role in determining the stability of the thin cooling layer that forms behind the bow shock. As seen in Figure 8, probably because of the axis-symmetric assumption in our simulations, the fastest growing mode in the unstable shock is a “dimple” forming along the axis of symmetry. Both the instability growth rate and the shock break up conditions may change given the additional degrees of freedom in three-dimensional simulations. For instance, the spherical accretion shock instability found in supernova simulations (e.g., Blondin & Shaw 2007) is less important in three-dimensional simulations than in 2D ones.

In this paper, as in the previous papers in this series, we assume that the radiation is emitted in a spherically symmetric manner near the BH. However, it is possible that the formation of optically thick structures near the BHs, such as an accretion disk, which are not resolved in our simulations, may change the angular dependence of the emitted radiation. For instance, Proga et al. (1998) have studied extensively the case of accretion on non-moving SMBHs in which UV photons are emitted preferentially in the direction perpendicular to the accretion disk. Here, we have not explored how such assump-

tion would affect our results for a moving BH. Neither we have explored the feedback effect from a collimated wind or jet, that may also develop in some phases of the BH accretion cycle.

Despite the aforementioned simplifying assumptions in our simulations, our results are a substantial improvement with respect to the Hoyle–Lyttleton model. The dependence of the growth rate and luminosity of BHs on their velocity with respect to the ambient gas is qualitatively modified by radiation feedback. The results reported in this paper may have significant repercussions in modeling and understanding the growth of stellar BHs in the early universe, the build up of an early X-ray background and provide important clues for explaining ULXs (Krolik, McKee, & Tarter 1981; Krolik & Kallman 1984; Krolik 2004; Ricotti & Ostriker 2004; Ri-

cotti, Ostriker, & Gnedin 2005; Ricotti 2007; Strohmayer & Mushotzky 2009; Volonteri & Bellovary 2012). We plan to address some of these issues in forthcoming papers.

The authors thank Richard Mushotzky, Chris Reynolds, Eve Ostriker, Tiziana Di Matteo, and James Drake for constructive comments and feedback. The numerical simulations presented in this paper were performed using high-performance computing clusters administered by the Center for Theory and Computation of the Department of Astronomy at the University of Maryland (“yorp”), and the Office of Information Technology at the University of Maryland (“deephought”). This research was supported by NASA grants NNX07AH10G and NNX10AH10G and NSF CMMI1125285. We thank the anonymous referee for constructive comments.

REFERENCES

- Abel, T., Anninos, P., Norman, M. L., & Zhang, Y. 1998, *ApJ*, 508, 518
 Abel, T., Bryan, G. L., & Norman, M. L. 2000, *ApJ*, 540, 39
 Alvarez, M. A., Wise, J. H., & Abel, T. 2009, *ApJ*, 701, L133
 Begelman, M. C. 1985, *ApJ*, 297, 492
 Begelman, M. C., Volonteri, M., & Rees, M. J. 2006, *MNRAS*, 370, 289
 Benensohn, J. S., Lamb, D. Q., & Taam, R. E. 1997, *ApJ*, 478, 723
 Bisnovatyi-Kogan, G. S., & Blinnikov, S. I. 1980, *MNRAS*, 191, 711
 Blecha, L., Cox, T. J., Loeb, A., & Hernquist, L. 2011, *MNRAS*, 412, 2154
 Blecha, L., Loeb, A., & Narayan, R. 2013, *MNRAS*, 429, 2594
 Blondin, J. M., Kallman, T. R., Fryxell, B. A., & Taam, R. E. 1990, *ApJ*, 356, 591
 Blondin, J. M., & Pope, T. C. 2009, *ApJ*, 700, 95
 Blondin, J. M., & Raymer, E. 2012, *ApJ*, 752, 30
 Blondin, J. M., & Shaw, S. 2007, *ApJ*, 656, 366
 Bondi, H. 1952, *MNRAS*, 112, 195
 Bondi, H., & Hoyle, F. 1944, *MNRAS*, 104, 273
 Bromm, V., Coppi, P. S., & Larson, R. B. 1999, *ApJ*, 527, L5
 Carr, B. J., Bond, J. R., & Arnett, W. D. 1984, *ApJ*, 277, 445
 Ciotti, L., & Ostriker, J. P. 2001, *ApJ*, 551, 131
 —. 2007, *ApJ*, 665, 1038
 Ciotti, L., Ostriker, J. P., & Proga, D. 2009, *ApJ*, 699, 89
 Cowie, L. L. 1977, *MNRAS*, 180, 491
 Cowie, L. L., Ostriker, J. P., & Stark, A. A. 1978, *ApJ*, 226, 1041
 Di Matteo, T., Colberg, J., Springel, V., Hernquist, L., & Sijacki, D. 2008, *ApJ*, 676, 33
 Di Matteo, T., Springel, V., & Hernquist, L. 2005, *Nature*, 433, 604
 Foglizzo, T., Galletti, P., & Ruffert, M. 2005, *A&A*, 435, 397
 Foglizzo, T., & Ruffert, M. 1997, *A&A*, 320, 342
 —. 1999, *A&A*, 347, 901
 Fryer, C. L., Woosley, S. E., & Heger, A. 2001, *ApJ*, 550, 372
 Fryxell, B. A., & Taam, R. E. 1988, *ApJ*, 335, 862
 Greif, T. H., Johnson, J. L., Klessen, R. S., & Bromm, V. 2008, *MNRAS*, 387, 1021
 Haehnelt, M. G., Natarajan, P., & Rees, M. J. 1998, *MNRAS*, 300, 817
 Hayes, J. C., Norman, M. L., Fiedler, R. A., Bordner, J. O., Li, P. S., Clark, S. E., ud-Doula, A., & Mac Low, M.-M. 2006, *ApJS*, 165, 188
 Hoyle, F., & Lyttleton, R. A. 1939, in *Proceedings of the Cambridge Philosophical Society*, Vol. 35, *Proceedings of the Cambridge Philosophical Society*, 405–4
 Jeon, M., Pawlik, A. H., Greif, T. H., Glover, S. C. O., Bromm, V., Milosavljević, M., & Klessen, R. S. 2012, *ApJ*, 754, 34
 Johnson, J. L., Khochfar, S., Greif, T. H., & Durier, F. 2011, *MNRAS*, 410, 919
 Johnson, J. L., Whalen, D. J., Fryer, C. L., & Li, H. 2012a, *ApJ*, 750, 66
 Johnson, J. L., Whalen, D. J., Li, H., & Holz, D. E. 2012b, *arXiv:1211.0548*
 Kim, J.-h., Wise, J. H., Alvarez, M. A., & Abel, T. 2011, *ApJ*, 738, 54
 Koide, H., Matsuda, T., & Shima, E. 1991, *MNRAS*, 252, 473
 Krolik, J. H. 2004, *ApJ*, 615, 383
 Krolik, J. H., & Kallman, T. R. 1984, *ApJ*, 286, 366
 Krolik, J. H., & London, R. A. 1983, *ApJ*, 267, 18
 Krolik, J. H., McKee, C. F., & Tarter, C. B. 1981, *ApJ*, 249, 422
 Kurosawa, R., & Proga, D. 2009a, *MNRAS*, 397, 1791
 —. 2009b, *ApJ*, 693, 1929
 Kurosawa, R., Proga, D., & Nagamine, K. 2009, *ApJ*, 707, 823
 Li, Y. 2011, *arXiv:1109.3442*
 Livio, M., Soker, N., Matsuda, T., & Anzer, U. 1991, *MNRAS*, 253, 633
 Lusso, E., & Ciotti, L. 2011, *A&A*, 525, A115
 Madau, P., & Rees, M. J. 2001, *ApJ*, 551, L27
 Matsuda, T., Inoue, M., & Sawada, K. 1987, *MNRAS*, 226, 785
 Matsuda, T., Sekino, N., Sawada, K., Shima, E., Livio, M., Anzer, U., & Boerner, G. 1991, *A&A*, 248, 301
 Mayer, L., Kazantzidis, S., Escala, A., & Callegari, S. 2010, *Nature*, 466, 1082
 Miller, M. C., & Colbert, E. J. M. 2004, *International Journal of Modern Physics D*, 13, 1
 Milosavljević, M., Bromm, V., Couch, S. M., & Oh, S. P. 2009a, *ApJ*, 698, 766
 Milosavljević, M., Couch, S. M., & Bromm, V. 2009b, *ApJ*, 696, L146
 Novak, G. S., Ostriker, J. P., & Ciotti, L. 2011, *ApJ*, 737, 26
 —. 2012, *MNRAS*, 427, 2734
 Oh, S. P., & Haiman, Z. 2002, *ApJ*, 569, 558
 Omukai, K., Schneider, R., & Haiman, Z. 2008, *ApJ*, 686, 801
 Ostriker, J. P., Choi, E., Ciotti, L., Novak, G. S., & Proga, D. 2010, *ApJ*, 722, 642
 Ostriker, J. P., Weaver, R., Yahil, A., & McCray, R. 1976, *ApJ*, 208, L61
 Park, K., & Ricotti, M. 2011, *ApJ*, 739, 2
 —. 2012, *ApJ*, 747, 9
 Pelupessy, F. I., Di Matteo, T., & Ciardi, B. 2007, *ApJ*, 665, 107
 Pogorelov, N. V., Ohsugi, Y., & Matsuda, T. 2000, *MNRAS*, 313, 198
 Proga, D. 2007, *ApJ*, 661, 693
 Proga, D., Ostriker, J. P., & Kurosawa, R. 2008, *ApJ*, 676, 101
 Proga, D., Stone, J. M., & Drew, J. E. 1998, *MNRAS*, 295, 595
 Regan, J. A., & Haehnelt, M. G. 2009, *MNRAS*, 396, 343
 Ricotti, M. 2007, *ApJ*, 662, 53
 Ricotti, M., Gnedin, N. Y., & Shull, J. M. 2001, *ApJ*, 560, 580
 Ricotti, M., & Ostriker, J. P. 2004, *MNRAS*, 352, 547
 Ricotti, M., Ostriker, J. P., & Gnedin, N. Y. 2005, *MNRAS*, 357, 207
 Ricotti, M., Ostriker, J. P., & Mack, K. J. 2008, *ApJ*, 680, 829
 Ruffert, M. 1996, *A&A*, 311, 817
 —. 1999, *A&A*, 346, 861
 Ruffert, M., & Arnett, D. 1994, *ApJ*, 427, 351
 Sazonov, S. Y., Ostriker, J. P., Ciotti, L., & Sunyaev, R. A. 2005, *MNRAS*, 358, 168
 Schneider, R., Ferrara, A., Natarajan, P., & Omukai, K. 2002, *ApJ*, 571, 30
 Shakura, N. I., & Sunyaev, R. A. 1973, *A&A*, 24, 337
 Shapiro, S. L. 1973, *ApJ*, 180, 531
 Shima, E., Matsuda, T., Anzer, U., Boerner, G., & Boffin, H. M. J. 1998, *A&A*, 337, 311
 Shima, E., Matsuda, T., Takeda, H., & Sawada, K. 1985, *MNRAS*, 217, 367
 Soker, N. 1990, *ApJ*, 358, 545
 Spitzer, L. 1978, *Physical Processes in the Interstellar Medium* (New York: Wiley)
 Springel, V., Di Matteo, T., & Hernquist, L. 2005, *MNRAS*, 361, 776
 Stacy, A., Greif, T. H., & Bromm, V. 2012, *MNRAS*, 422, 290
 Stone, J. M., & Norman, M. L. 1992, *ApJS*, 80, 753
 Strohmayer, T. E., & Mushotzky, R. F. 2009, *ApJ*, 703, 1386
 Taam, R. E., & Fryxell, B. A. 1988, *ApJ*, 327, L73
 van der Marel, R. P. 2004, *Coevolution of Black Holes and Galaxies*, 37
 Vishniac, E. T. 1994, *ApJ*, 428, 186
 Vitello, P. 1984, *ApJ*, 284, 394
 Volonteri, M., & Bellovary, J. 2012, *Reports on Progress in Physics*, 75, 124901
 Volonteri, M., Lodato, G., & Natarajan, P. 2008, *MNRAS*, 383, 1079
 Volonteri, M., & Rees, M. J. 2005, *ApJ*, 633, 624
 Wandel, A., Yahil, A., & Milgrom, M. 1984, *ApJ*, 282, 53
 Whalen, D., & Norman, M. L. 2006, *ApJS*, 162, 281
 —. 2008a, *ApJ*, 673, 664
 Whalen, D. J., & Fryer, C. L. 2012, *ApJ*, 756, L19
 Whalen, D. J., & Norman, M. L. 2008b, *ApJ*, 672, 287
 —. 2011, *Ap&SS*, 336, 169
 Wheeler, J. C., & Johnson, V. 2011, *ApJ*, 738, 163
 Zarinelli, A., Walder, R., & Nussbaumer, H. 1995, *A&A*, 301, 922